LETTER

doi:10.1038/nature21695

Cytosolic proteostasis through importing of misfolded proteins into mitochondria

Linhao Ruan[1,2]*, Chuankai Zhou[3]*, Erli Jin[2], Andrei Kucharavy[1,2], Ying Zhang[3], Zhihui Wen[3], Laurence Florens[3] & Rong Li[1,2]

Loss of proteostasis underlies ageing and neurodegeneration characterized by the accumulation of protein aggregates and mitochondrial dysfunction[1–5]. Although many neurodegenerative-disease-associated proteins can be found in mitochondria[4,6], it remains unclear how mitochondrial dysfunction and protein aggregation could be related. In dividing yeast cells, protein aggregates that form under stress or during ageing are preferentially retained by the mother cell, in part through tethering to mitochondria, while the disaggregase Hsp104 helps to dissociate aggregates and thereby enables refolding or degradation of misfolded proteins[7–10]. Here we show that, in yeast, cytosolic proteins prone to aggregation are imported into mitochondria for degradation. Protein aggregates that form under heat shock contain both cytosolic and mitochondrial proteins and interact with the mitochondrial import complex. Many aggregation-prone proteins enter the mitochondrial intermembrane space and matrix after heat shock, and some do so even without stress. Timely dissolution of cytosolic aggregates requires the mitochondrial import machinery and proteases. Blocking mitochondrial import but not proteasome activity causes a marked delay in the degradation of aggregated proteins. Defects in cytosolic Hsp70s leads to enhanced entry of misfolded proteins into mitochondria and elevated mitochondrial stress. We term this mitochondria-mediated proteostasis mechanism MAGIC (mitochondria as guardian in cytosol) and provide evidence that it may exist in human cells.

We developed an affinity-based method, using the model aggregation substrate GFP- and Flag-tagged luciferase[11] (FlucSM–GFP–3× Flag), to purify protein aggregates induced by heat shock and to identify their components using quantitative multi-dimensional protein identification technology (MudPIT) to compare the experimental strain with the control lacking the Flag tag (Extended Data Fig. 1a–c). We identified 319 proteins that were substantially enriched with false discovery rate (FDR) < 0.05 in heat-shock-induced aggregates (Supplementary Tables 1, 2). These proteins are referred to as aggregate proteins hereafter. Forty-five per cent of aggregate proteins were observed to form visible aggregates after heat shock by using available GFP-tagged strains (Extended Data Fig. 1d). Eighteen per cent of aggregate proteins found in our study overlapped with those identified previously using differential centrifugation[12]. Gene ontology revealed that aggregate proteins were significantly enriched ($P < 0.05$) for proteasome components, chaperones, RNA-binding proteins, stress granules, and mitochondrial proteins (Fig. 1a).

Tom70 and Tom40, two mitochondrial outer membrane proteins involved in import[13], were among the mitochondrial proteins that co-purified with aggregates. Microscopy revealed that Tom70–GFP was evenly distributed on the mitochondrial membrane, rather than colocalizing with aggregates (Extended Data Fig. 1e), but the biochemical interaction of Tom70 and Tom40 with aggregates was verified (Extended Data Fig. 1f, g). Chlorophenylhydrazone (CCCP), which disrupts the mitochondrial membrane potential required for import[14], but not antimycin, which blocks mitochondrial ATP production, prevents the dissolution of Hsp104–GFP-labelled aggregates[9]. CCCP also disrupted the dissolution of FlucSM–GFP aggregates in the presence of cycloheximide (CHX), without depleting cellular ATP[15,16] (Extended Data Fig. 1h, i). We therefore hypothesized that aggregate dissolution involves the import of aggregate proteins into mitochondria. To test this hypothesis, we compared the dissolution kinetics of heat-shock aggregates in cells expressing wild-type *TIM23* (encoding a subunit of the mitochondrial inner membrane import complex) or the temperature-sensitive mutant *tim23ts* (refs 13, 17). *tim23*^{ts} was inactivated during heat shock and prevented aggregate dissolution after shifting back to 23 °C in the presence of CHX (Fig. 1b, c), and this effect was not due to disruption of mitochondrial membrane potential (Extended Data Fig. 1j).

To visualize the entry of aggregate proteins into mitochondria, we employed the split GFP system[18] where the first ten β-strands of GFP ($GFP_{1–10}$), linked with mCherry, were targeted to mitochondria through linkage with a mitochondria-targeting sequence[19] (MTS–mCherry–$GFP_{1–10}$), while the eleventh β-strand (GFP_{11}) was linked with an aggregate protein (Extended Data Fig. 2a). Mitochondrial GFP fluorescence was expected only if the GFP_{11}-linked protein entered mitochondria. For positive and negative controls, GFP_{11}-tagged Grx5, a mitochondrial matrix protein, showed a prominent mitochondrial split-GFP signal, whereas GFP_{11}-tagged Hsp104 or the non-aggregate cytosolic protein Not3 (Extended Data Fig. 1d) showed no mitochondrial split-GFP signal with or without heat shock (Extended Data Fig. 2b). GFP_{11}-tagged aggregate proteins, including FlucSM and several native aggregate proteins, showed no or low-level mitochondrial GFP fluorescence before heat shock, but after heat shock the mitochondrial split-GFP signal increased strongly (Fig. 2a–c; Extended Data Fig. 2c), and this increase could be prevented by CCCP (Extended Data Fig. 2d–f). Structured illumination microscopy (SIM), applied to a strain in which the mitochondrial outer membrane was labelled with mCherry–Fis1TM[9] and $GFP_{1–10}$ was targeted into mitochondria by linking to Grx5, confirmed that the split GFP signal of Lsg1–GFP11 was inside mitochondria (Fig. 2d, Supplementary Video 1). Mitochondrial import under heat shock was also observed for TDP-43 expressed in yeast, a protein associated with several forms of neurodegeneration[20] (Extended Data Fig. 2g, h). Notably, deletions of the stress-associated genes *SSA2*, *SSA3* and *SSA4* together with expression of a temperature-sensitive *ssa1*^{ts} mutant[21] (*Δssa2 Δssa3 Δssa4 ssa1*^{ts}) disrupted cytosolic Hsp70 proteins and led to the import of FlucSM with or without heat shock (Fig. 2e), whereas disrupting Hsp104 activity with GdnHCl[22] reduced the amount of imported FlucSM–GFP_{11} (Extended Data Fig. 2i, j), suggesting that Hsp104 but not Hsp70 is involved in mitochondrial import of aggregate proteins.

To examine the import of aggregate proteins into mitochondria biochemically, we purified mitochondria from cells expressing

[1]Center for Cell Dynamics, Department of Cell Biology, Johns Hopkins University School of Medicine, 855 North Wolfe Street, Baltimore, Maryland 21205, USA. [2]Department of Chemical and Biomolecular Engineering, Whiting School of Engineering, Johns Hopkins University, Baltimore, Maryland 21218, USA. [3]Stowers Institute for Medical Research, 1000 East 50th Street, Kansas City, Missouri 64110, USA.
*These authors contributed equally to this work.

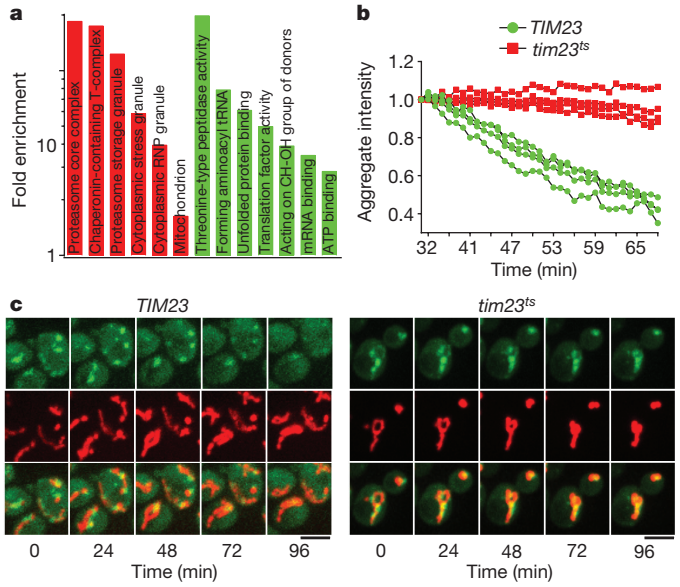

Figure 1 | Heat shock aggregates and mitochondrial import. **a**, Gene ontology enrichment of aggregate proteins. Green, molecular function; red, cellular components. **b**, Dissolution of aggregates, labelled with Hsp104–GFP, in *TIM23* (green) or *tim23*^{ts} cells (red). Shown are fluorescence traces from three biological repeats. **c**, Montage of movies used in **b**. Top, aggregates; middle, mitochondria; bottom, merged. Scale bars, 5 μm.

FlucSM–HA after heat shock. Sequential trypsin and protease K treatments were used to eliminate the substantial amount of aggregates attached to the outside of mitochondria (Extended Data Fig. 2k–m). The mitochondrial outer and inner membranes were permeabilized with digitonin and Triton X-100, respectively[23,24]. Immunoblots for FlucSM and markers of outer membrane (Tom70), intermembrane space (Dld1) and matrix (Abf2) showed that FlucSM was present in both the intermembrane space and the matrix (Extended Data Fig. 2l–n). As an alternative method, MTS–GFP–APEX2 (Extended Data Fig. 2o, p) was introduced into the strain with a native aggregate protein, Tma19, tagged with haemagglutinin at its genomic locus. After cell permeabilization, the mitochondrial matrix was briefly biotinylated, followed by extensive washes, removal of the mitochondrial inner membrane and affinity purification of biotinylated proteins. The aggregate protein Tma19–HA, but not the control (HA-tagged cytosolic Ppt1), was detected among the biotinylated proteins after but not before heat shock (Fig. 2f).

During recovery at normal temperature after heat shock, the split-GFP signal of aggregate proteins in mitochondria disappeared, with kinetics similar to the dissolution of cytosolic aggregates (Fig. 3a, b, Extended Data Fig. 3a, b, compared to Fig. 1b), suggesting that the degradation of aggregate proteins imported into mitochondria accompanied aggregate dissolution. To test this biochemically, we incubated aggregates purified from the strain expressing FlucSM–HA–GFP–3×Flag with protease inhibitors and purified mitochondria (labelled with mCherry). As expected, aggregates and mitochondria clustered together (Extended Data Fig. 3c). FlucSM–HA–GFP–3×Flag degradation was observed after 1.5 h of incubation, as shown by a marked decrease in the full-length protein accompanied by the appearance of a cleavage product, in reactions with wild-type mitochondria but not those without mitochondria or with mitochondria from *tim23*^{ts} mutant (Fig. 3c, Extended Data Fig. 3d). Furthermore, FlucSM–HA–GFP–3×Flag in aggregates purified from the *Δhsp104* strain was not degraded by wild-type mitochondria (Extended Data Fig. 3e, f). This result confirmed that degradation of FlucSM in aggregates required import-competent mitochondria and Hsp104.

We next screened the 13 non-essential mitochondrial proteases, processing peptidases or oligopeptidases[25] for their effect on the dissolution of heat shock aggregates. Deletion of *PIM1*, which encodes a LON protease, produced the strongest inhibitory effect (Extended Data Fig. 3g, h). To test the role of Pim1 further, we introduced into the genome the *pim1*^{S1015A} mutation, which disrupts the proteolytic activity of Pim1 (ref. 26). This mutant showed normal mitochondrial morphology and growth (Fig. 3a and Extended Data Fig. 4a, b), but the disappearance of the FlucSM split-GFP signal in mitochondria during recovery was delayed compared to wild-type cells without or with CHX, which prevented further production of aggregate proteins[9] (Fig. 3a, b, Extended Data Fig. 4c, d).

To estimate the contribution of mitochondrial import to the turnover of aggregate proteins relative to other mechanisms, we compared the degradation kinetics of FlucSM–HA and Lsg1–HA after heat shock in the

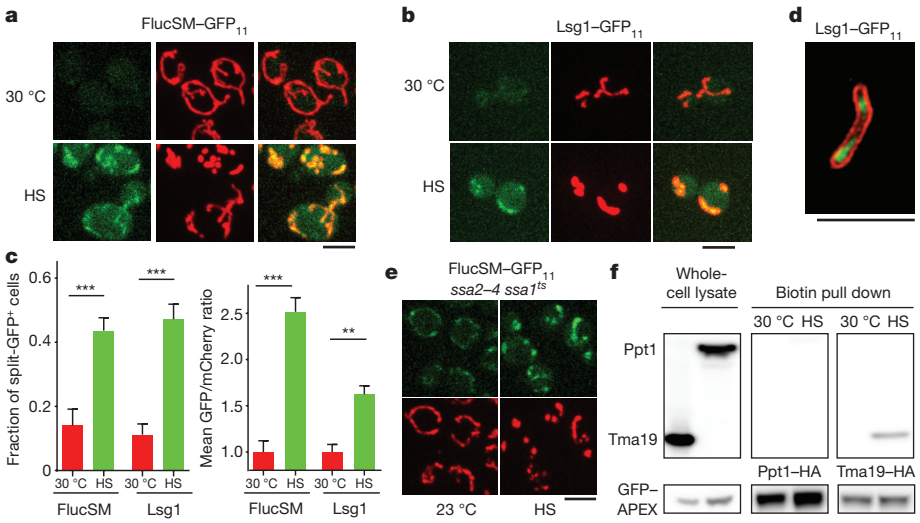

Figure 2 | Mitochondrial import of aggregate proteins. **a**, **b**, Images of cells expressing FlucSM–GFP$_{11}$ (**a**) and Lsg1–GFP$_{11}$ (**b**). Left, split GFP; middle, mitochondria; right, merged. **c**, Fractions of split-GFP^{+} cells and normalized mean GFP/mCherry ratio from experiments in **a** and **b**. Data are means and s.e.m. of (left to right) 209, 215, 252 and 235 (left graph) and 145, 147, 111 and 133 (right graph) cells imaged and quantified; three biological repeats. **d**, Merged SIM images after heat shock. Green, Lsg1 split-GFP; red, mCherry–Fis1TM. Three biological repeats, 21 cells imaged. **e**, Images with FlucSM–GFP$_{11}$ split-GFP (top) and mitochondria (bottom). Quantification in Extended Data Fig. 2j. Three biological repeats. **f**, Anti-HA immunoblot of whole-cell lysate and proteins biotinylated by MTS–GFP–APEX2. Unpaired two-tailed *t*-test for **c**: $^{**}P < 0.01$, $^{***}P < 0.001$. Scale bars, 5 μm. For gel source data, see Supplementary Fig. 1. HS, heat shock.

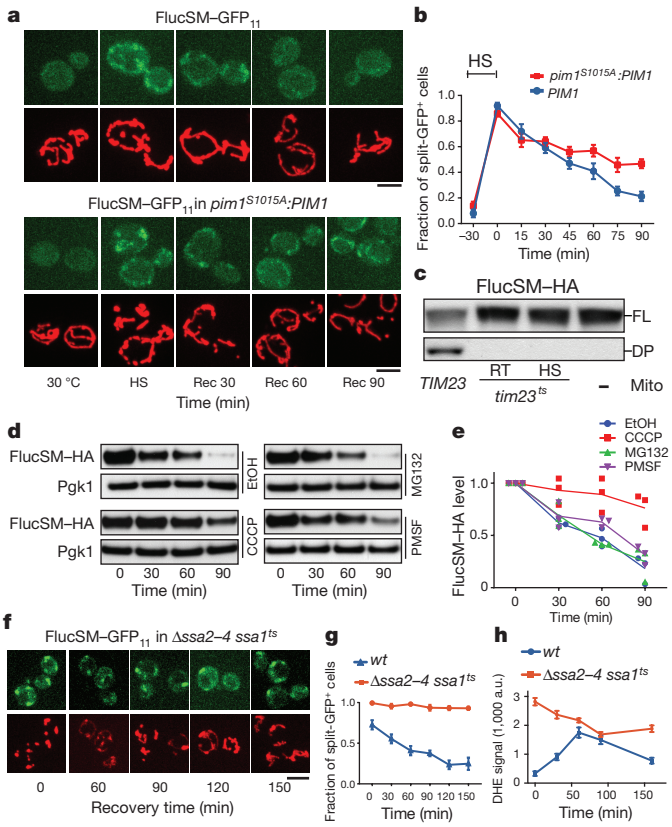

Figure 3 | Degradation of aggregate proteins in mitochondria. **a**, **b**, Images (**a**) and quantification (**b**) of FlucSM–GFP_{11} split-GFP signal in wild-type (top set) and *pim1*^{S1015A}*:PIM1* (bottom set) during recovery after heat shock. Bottom images in each panel show mitochondria. Shown in **b**: mean and s.e.m. of 1,643 wild type and 1,805 *pim1*^{S1015A}*:PIM1* cells imaged and quantified; three biological repeats. **c**, Immunoblots of FlucSM–HA after aggregates incubated for 90 min with or without *TIM23* or *tim23*^{ts} mitochondria as indicated. RT, room temperate; FL, full length; DP, degradation product. **d**, **e**, Immunoblots (**d**) and quantification (**e**), showing data points and mean plots from three biological repeats, of FlucSM–HA degradation *in vivo* in the presence of indicated agents. **f**, **g**, Images (**f**, organized as in **a**) and quantification (**g**) of FlucSM split-GFP signal in *Δssa2 Δssa3 Δssa4 ssa1*^{ts} cells during recovery after heat shock. Shown in (**g**): mean and s.e.m. of 244, 253, 295, 163, 196 and 209 mutant and 174, 218, 221, 197, 203 and 280 wild-type cells imaged and quantified; three biological repeats. **h**, Quantification of ROS with dihydroethidium (DHE) staining. Shown: mean and s.e.m. of 1,621 mutant and 2,151 wild-type cells imaged and quantified; two biological repeats. Scale bars, 5 μm. For gel source data, see Supplementary Fig. 1.

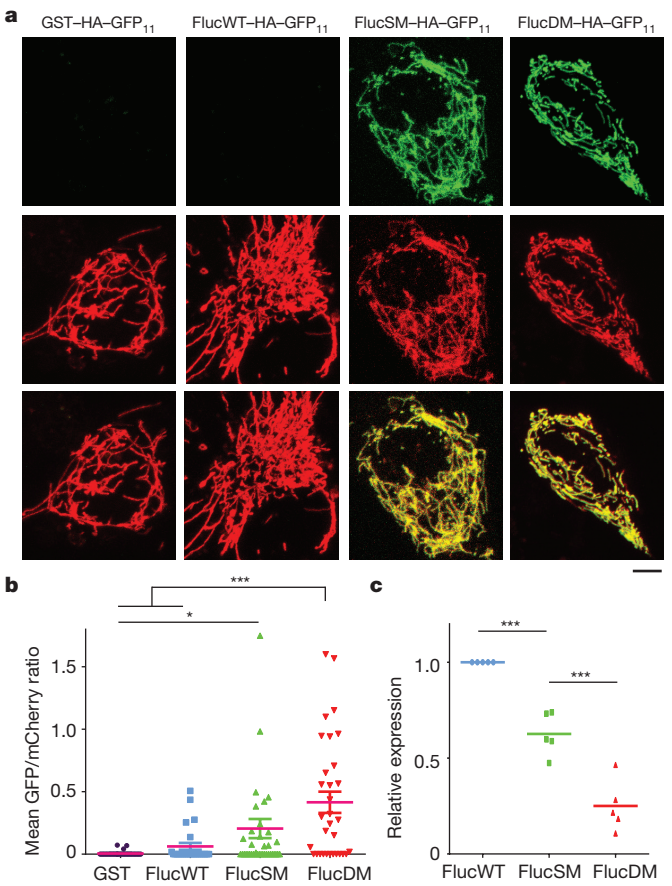

Figure 4 | Mitochondrial import of unstable proteins in RPE1 cells. **a**, Images of mitochondria (middle) and split-GFP (top) of GFP_{11}-tagged proteins in RPE1 cells. Bottom, merged. **b**, Quantification of normalized GFP/mCherry ratio in a field. Pink line, mean; 34, 26, 39 and 32 fields quantified. Dunn's multiple comparisons test, none parametric. Three biological repeats. **c**, Expression of luciferase proteins normalized to FlucWT. Shown: data points and mean of five biological repeats. Tukey's multiple comparisons test: $***P < 0.001$; $*P < 0.05$. Scale bars, 5 μm.

presence of CHX combined with MG132 (inhibiting the proteasome), phenylmethylsulfonyl fluoride (PMSF, inhibiting serine proteases in the vacuole), or CCCP, in the *Δpdr5* strain with enhanced drug permeability[27,28]. CCCP strongly delayed the degradation of FlucSM and Lsg1 after heat shock (Fig. 3d, e, Extended Data Fig. 4e, f). Consistently, inhibition of import with *tim23*^{ts} also delayed FlucSM turnover after heat shock (Extended Data Fig. 4g, h). By contrast, MG132 had little effect on aggregate protein degradation after heat shock, even though the drug efficacy was confirmed by the inhibition of FlucSM degradation without heat shock (Extended Data Fig. 4i, j). PMSF moderately slowed the degradation of Lsg1 and FlucSM. This experiment shows that mitochondrial import makes a substantial contribution to the degradation of aggregate proteins after heat shock, whereas the lack of requirement for the proteasome is consistent with the observation that many proteasome components were enriched in aggregates after heat shock (Fig. 1a).

We next tested the effect of loss of cytosolic proteostasis in the *Δssa2 Δssa3 Δssa4 ssa1*^{ts} mutant on aggregate protein clearance inside mitochondria. The split GFP signal in this mutant persisted after shifting back to 23 °C (Fig. 3f, g), probably owing to continuous flow of misfolded FlucSM–GFP_{11} into mitochondria, as CHX treatment enabled the decay of the split-GFP signal (Extended Data Fig. 5a, b). Notably, this mutant also displayed much more severe and persistent fragmentation of mitochondria (Fig. 3f, Extended Data Fig. 5c) and high-level mitochondrial reactive oxidative species (ROS) compared to wild-type cells after heat shock (Fig. 3h, Extended Data Fig. 5d). These manifestations of mitochondrial stress have also been observed in neurodegenerative diseases[1,4,29].

Although most aggregate proteins tested were imported into mitochondria after heat shock, some, such as the RNA helicase Ded1, showed a prominent split-GFP signal in mitochondria even without heat shock (Extended Data Fig. 6a–d, and e for additional examples). Ded1 was previously classified as a super aggregator with a low stress threshold for aggregation[12]. After CCCP or CHX was added to prevent further import or synthesis, respectively, the split-GFP signal of Ded1, but not of the stable mitochondrial protein Grx5, diminished with time (Extended Data Figs 2b, 6a–d), suggesting that highly unstable cytosolic proteins are imported into and degraded in mitochondria even under physiological conditions. To test whether import of aggregation-prone proteins into mitochondria occurs in mammalian cells, we fused HA–GFP_{11} to wild-type luciferase (FlucWT) and two mutants, FlucSM and FlucDM, of which FlucDM has the highest structural instability[11]. Each construct, or GST–HA–GFP_{11} as another control for stable protein, was co-transfected with a plasmid expressing

MTS–mCherry–$GFP_{1–10}$ into human RPE1 cells. GST–HA–GFP_{11} or FlucWT–HA–GFP_{11} produced little or no split-GFP fluorescence, whereas FlucSM–HA–GFP_{11} and FlucDM–HA–GFP_{11} showed increasingly strong split-GFP fluorescence in mitochondria (Fig. 4a, b), even though the protein levels of FlucWT, FlucSM and FlucDM were in a decreasing order owing to instability of the mutants[11] (Fig. 4c, Extended Data Fig. 6f), suggesting that unstable aggregation-prone cytosolic proteins are also imported into mitochondria in human cells.

On the basis of these results, we speculate that protein aggregates engaged with mitochondria via interaction with import receptors such as Tom70, leading to import of aggregate proteins followed by degradation by mitochondrial proteases such as Pim1 (Extended Data Fig. 6g). The import of aggregate proteins appears not to require cytosolic Hsp70, but Hsp104 is involved, possibly by dissociating proteins from aggregates to enable their entry into import channels. As blocking mitochondrial import prevented disaggregation *in vivo*, the mitochondrial import process may facilitate disaggregation by actively removing dissociated proteins from aggregates, although we cannot rule out an indirect effect. While the mechanistic details of this process require further investigation, our findings establish mitochondria as an important guardian of cytosolic proteostasis and we term this mechanism MAGIC. In yeast, MAGIC appears to be crucial for the turnover of proteins that aggregate under stress. If this also happens in human cells, the accumulation of certain disease proteins in mitochondria[4] could reflect a general deficiency in cellular proteostasis[30]. A resulting overabundance of disease or misfolded proteins inside mitochondria could disrupt mitochondrial biosynthetic activities or overwhelm the proteostasis of mitochondria, leading to organelle dysfunction. On the other hand, the decline of mitochondrial fitness in ageing or disease could lead to diminished MAGIC owing to loss of membrane potential or protein degradation capacity, leading to impeded cytosolic proteostasis and buildup of protein aggregates.

Online Content Methods, along with any additional Extended Data display items and Source Data, are available in the online version of the paper; references unique to these sections appear only in the online paper.

Received 19 June 2016; accepted 9 February 2017.
Published online 1 March 2017.

1. Lin, M. T. & Beal, M. F. Mitochondrial dysfunction and oxidative stress in neurodegenerative diseases. *Nature* **443,** 787–795 (2006).
2. Balch, W. E., Morimoto, R. I., Dillin, A. & Kelly, J. W. Adapting proteostasis for disease intervention. *Science* **319,** 916–919 (2008).
3. Hartl, F. U., Bracher, A. & Hayer-Hartl, M. Molecular chaperones in protein folding and proteostasis. *Nature* **475,** 324–332 (2011).
4. Schapira, A. H. Mitochondrial diseases. *Lancet* **379,** 1825–1834 (2012).
5. López-Otín, C., Blasco, M. A., Partridge, L., Serrano, M. & Kroemer, G. The hallmarks of aging. *Cell* **153,** 1194–1217 (2013).
6. Hansson Petersen, C. A. *et al.* The amyloid β-peptide is imported into mitochondria via the TOM import machinery and localized to mitochondrial cristae. *Proc. Natl Acad. Sci. USA* **105,** 13145–13150 (2008).
7. Parsell, D. A., Kowal, A. S., Singer, M. A. & Lindquist, S. Protein disaggregation mediated by heat-shock protein Hsp104. *Nature* **372,** 475–478 (1994).
8. Doyle, S. M., Genest, O. & Wickner, S. Protein rescue from aggregates by powerful molecular chaperone machines. *Nat. Rev. Mol. Cell Biol.* **14,** 617–629 (2013).
9. Zhou, C. *et al.* Organelle-based aggregation and retention of damaged proteins in asymmetrically dividing cells. *Cell* **159,** 530–542 (2014).
10. Miller, S. B., Mogk, A. & Bukau, B. Spatially organized aggregation of misfolded proteins as cellular stress defense strategy. *J. Mol. Biol.* **427,** 1564–1574 (2015).
11. Gupta, R. *et al.* Firefly luciferase mutants as sensors of proteome stress. *Nat. Methods* **8,** 879–884 (2011).
12. Wallace, E. W. *et al.* Reversible, specific, active aggregates of endogenous proteins assemble upon heat stress. *Cell* **162,** 1286–1298 (2015).
13. Neupert, W. & Herrmann, J. M. Translocation of proteins into mitochondria. *Annu. Rev. Biochem.* **76,** 723–749 (2007).
14. Martin, J., Mahlke, K. & Pfanner, N. Role of an energized inner membrane in mitochondrial protein import. ΔΨ drives the movement of presequences. *J. Biol. Chem.* **266,** 18051–18057 (1991).
15. Serrano, R. Energy requirements for maltose transport in yeast. *Eur. J. Biochem.* **80,** 97–102 (1977).
16. Stevens, H. C. & Nichols, J. W. The proton electrochemical gradient across the plasma membrane of yeast is necessary for phospholipid flip. *J. Biol. Chem.* **282,** 17563–17567 (2007).
17. Pareek, G., Krishnamoorthy, V. & D'Silva, P. Molecular insights revealing interaction of Tim23 and channel subunits of presequence translocase. *Mol. Cell. Biol.* **33,** 4641–4659 (2013).
18. Cabantous, S., Terwilliger, T. C. & Waldo, G. S. Protein tagging and detection with engineered self-assembling fragments of green fluorescent protein. *Nat. Biotechnol.* **23,** 102–107 (2005).
19. Fehrenbacher, K. L., Yang, H. C., Gay, A. C., Huckaba, T. M. & Pon, L. A. Live cell imaging of mitochondrial movement along actin cables in budding yeast. *Curr. Biol.* **14,** 1996–2004 (2004).
20. Lagier-Tourenne, C., Polymenidou, M. & Cleveland, D. W. TDP-43 and FUS/TLS: emerging roles in RNA processing and neurodegeneration. *Hum. Mol. Genet.* **19** (R1), R46–R64 (2010).
21. Becker, J., Walter, W., Yan, W. & Craig, E. A. Functional interaction of cytosolic hsp70 and a DnaJ-related protein, Ydj1p, in protein translocation *in vivo*. *Mol. Cell. Biol.* **16,** 4378–4386 (1996).
22. Kummer, E., Oguchi, Y., Seyffer, F., Bukau, B. & Mogk, A. Mechanism of Hsp104/ClpB inhibition by prion curing guanidinium hydrochloride. *FEBS Lett.* **587,** 810–817 (2013).
23. Ryan, M. T., Voos, W. & Pfanner, N. Assaying protein import into mitochondria. *Methods Cell Biol.* **65,** 189–215 (2001).
24. Devi, L., Raghavendran, V., Prabhu, B. M., Avadhani, N. G. & Anandatheerthavarada, H. K. Mitochondrial import and accumulation of α-synuclein impair complex I in human dopaminergic neuronal cultures and Parkinson disease brain. *J. Biol. Chem.* **283,** 9089–9100 (2008).
25. Baker, M. J., Tatsuta, T. & Langer, T. Quality control of mitochondrial proteostasis. *Cold Spring Harb. Perspect. Biol.* **3,** a007559 (2011).
26. Rep, M. *et al.* Promotion of mitochondrial membrane complex assembly by a proteolytically inactive yeast Lon. *Science* **274,** 103–106 (1996).
27. Lee, D. H. & Goldberg, A. L. Selective inhibitors of the proteasome-dependent and vacuolar pathways of protein degradation in *Saccharomyces cerevisiae*. *J. Biol. Chem.* **271,** 27280–27284 (1996).
28. Collins, G. A., Gomez, T. A., Deshaies, R. J. & Tansey, W. P. Combined chemical and genetic approach to inhibit proteolysis by the proteasome. *Yeast* **27,** 965–974 (2010).
29. Knott, A. B., Perkins, G., Schwarzenbacher, R. & Bossy-Wetzel, E. Mitochondrial fragmentation in neurodegeneration. *Nat. Rev. Neurosci.* **9,** 505–518 (2008).
30. Tyedmers, J., Mogk, A. & Bukau, B. Cellular strategies for controlling protein aggregation. *Nat. Rev. Mol. Cell Biol.* **11,** 777–788 (2010).

Supplementary Information is available in the online version of the paper.

Acknowledgements The authors thank K. Si for technical advice and reagents, and F.-U. Hartl, E. Craig, P. Silva, B. Bukau, S. Claypool and J. Wang for reagents. This work was supported by the grant R35 GM118172 from the National Institute of Health to R.L., and a fellowship from the American Heart Association to C.Z.

Author Contributions L.R.: split-GFP experiments, biochemical assays with purified mitochondria (assisted by E.J.), all protein degradation experiments, aggregate dissolution in protease mutants, manuscript preparation; C.Z.: aggregate purification for proteomics, APEX experiments, aggregate dissolution in *tim23*^{ts}, measurement of mitochondrial ROS, manuscript preparation; E.J.: validation of proteomics candidates, split-GFP imaging repeats and quantification, growth assays; A.K.: image quantification programs and data analysis; Y.Z., Z.W. and L.F.: MudPIT proteomics; R.L.: overall project supervision and manuscript preparation.

Author Information Reprints and permissions information is available at www.nature.com/reprints. The authors declare no competing financial interests. Readers are welcome to comment on the online version of the paper. Publisher's note: Springer Nature remains neutral with regard to jurisdictional claims in published maps and institutional affiliations. Correspondence and requests for materials should be addressed to R.L. (rong@jhu.edu).

METHODS

Yeast strains and plasmids. Yeast strains used in this study are based on the BY4741 background as listed in Supplementary Table 3. The *ssa1*^{ts} strain was a gift from E. Craig's laboratory. The *tim23*^{ts} strain was a gift from P. Silva's laboratory. Gene deletion and HA, GFP_{11} and GFP tagging were performed with PCR-mediated homologous recombination[31] and correct integrations were confirmed by PCR. The *pim1*^{S1015A}*:PIM1* mutant was constructed by integration of the plasmid carrying *pim1*^{S1015A} under the *PIM1* promoter into the *PIM1* locus. Plasmids containing FlucWT, FlucSM and FlucDM were constructed using plasmids provided by F.-U. Hartl[11]. pRS306–LuciYFP was a gift from B. Bukau. The Tdp43 plasmid was a gift from J. Wang's laboratory. Most of the expression plasmids were constructed using the p404 backbone[32]. MudPIT hits were verified with strains from the yeast GFP library[33]. DNA fragments for the split-GFP system were synthesized by gBlocks[18]. GFP1–10 was in frame with the mitochondria targeting sequence (MTS) and mCherry. GFP_{11} replaced GFP in pFA6a–GFP(S65T)–$His_3M\times6$ to serve as the universal C-terminal tagging plasmid. APEX2 was in frame with MTS–GFP. For the SIM assay, the mitochondrial outer membrane was labelled with mCherry–Fis1TM[9]; $GFP_{1–10}$ was fused with the mitochondrial matrix protein Grx5 (Grx5– $GFP_{1–10}$); and the native aggregate protein Lsg1 was tagged with GFP_{11}. For mammalian plasmids, MTS–mCherry–$GFP_{1–10}$ replaced the DsRed in pDsRed-Monomer-Hyg-N1 vector; GST–HA–GFP_{11}, FlucWT–HA–GFP_{11}, FlucSM–HA–GFP_{11} or FlucDM–HA–GFP_{11} replaced the GFP in pAcGFP1-N1 vector.

Confocal microscopy. Live-cell images of yeast were acquired using a Yokagawa CSU-10 spinning disc on the side port of a Carl Zeiss 200 m inverted microscope or a Perkin Elmer Ultraview VoX system equipped with Zeiss Definite Focus, or a Carl Zeiss LSM-510 Confocor 3 system. 488 or 561 nm excitation was used to excite green or red fluorescent proteins, respectively, and emission was collected through the appropriate filters onto a Hamamatsu C9100-13 EMCCD on the spinning disc systems or the single photon avalanche photodiodes on the Confocor 3. All GFP images were acquired through a 500–550 nm filter. RFP images were acquired with a 580 nm long pass filter on the CSU-10, and a 420–475/502–544/582–618/663–691 multiband filter on the Ultraview. All images were acquired in a multi-track, alternating excitation configuration so as to avoid GFP bleed-through. The CSU-10 and Ultraview systems used a 100× 1.45 NA Plan-Apochromat objective. Images were acquired using MetaMorph (version 7.0; MDS Analytical Technologies) on CSU-10 spinning disc system, Volocity 6.3 (Perkin Elmer) on Ultraview system and Carl Zeiss AIM software for the LSM 510. Mammalian cell images were acquired using Zeiss LSM780 confocal with a 40×/1.4 oil Plan-Apochromat objective.

Yeast cells were grown in synthetic complete (SC) or drop-out medium containing 2% dextrose overnight at 30 °C (23 °C for temperature-sensitive mutants). The 4 ml (or 8 ml for recovery assays) mid-log culture with an OD_{600} of roughly 0.5 was transferred to 42 °C to be heat-shocked for 30 min. For 3D fluorescence time-lapse imaging, cells were placed on a thin SC (2% dextrose) agarose gel pad to allow prolonged imaging at room temperature[34]. 3D image stacks were acquired every minute for 60–90 min. Each *z* series was acquired with a 0.5 μm step size. All image processing was performed using the Image J software (NIH). For visualization purposes, images in the figure were scaled with bilinear interpolation.

Drug treatments and antibodies. Cycloheximide (C4859, Sigma) was added to a final concentration of 100 μg/ml. Hydrogen peroxide solution (216763, Sigma) was diluted 10 times in H_2O and added to a final concentration of 0.7 mM at 30 °C to induce protein aggregation. CCCP (C2759, Sigma) was dissolved in DMSO or ethanol to 20 mM as stock and 25 μM was used to treat cells. MG132 (c2211, Sigma) was dissolved in DMSO and 80 μM was used to treat cells. PMSF (P7626, Sigma) was dissolved in ethanol and 1 mM was used to treat cells. DHE staining was done by incubating cells with 180 μM DHE (D11347, Invitrogen) for 10 min at room temperature. Tetramethylrhodamine methyl ester perchlorate (TMRM, T5428, Sigma) was added to a final concentration of 1 μM for 30 min at 30 °C. Anti-HA-peroxidase for the APEX assay was obtained from Sigma (12013819001). HA-tag (C29F4) rabbit mAb #3724 from Cell Signaling Technique was used for all the other immunoblots. Anti-GFP was from MBL International Corporation (#598). Guanidine hydrochloride (Sigma G3272; 3 mM) was added during heat shock. Anti-Tom70 antibody, anti-Dld1 antibody and anti-Abf2 antibody were provided by S. Claypool's laboratory.

Aggregate dissolution assay. Aggregate dissolution assays were carried out as described previously[35]. In brief, yeast cells were heat shocked at 42 °C for 30 min and recovered for 15 min at 30 °C or 23 °C (for temperature-sensitive mutants) with or without additional drugs such as CHX or CCCP before being mounted on an agarose gel-pad slide for 3D time-lapse imaging. The major technical flow is as follows: masks of the aggregates were generated, and then cell areas and cytoplasm were created and used to calculate the average intensity of aggregate regions (including cytosolic background), average cytosolic intensity, and total aggregate area. The average cytosolic intensity was subtracted from the average aggregate region intensity to obtain the corrected average aggregate intensity without cytosolic background. Finally, the total aggregate intensity was calculated by multiplying the corrected average aggregate intensity by the aggregate area and normalizing it to the initial intensity for comparison between strains or conditions. Aggregate intensities were measured starting 30 min after the start of acquisition because, during the early part of the movies, aggregates grew in intensity as explained in detail previously[35].

Measurement of cellular ATP using FRET-based biosensor. Fluorescence resonance energy transfer (FRET) measurement of cellular ATP was performed using the acceptor photobleaching method as described previously[9]. In brief, yeast cells expressing AT1.03[36] were heat-shocked at 42 °C for 30 min and recovered with or without the indicated compounds for 0, 30 or 60 min. Cells were then immobilized on a glass slide and imaged using a Perkin-Elmer Ultraview spinning disc system with a CSU-X1 Yokogawa disc. A 100× 1.4 NA plan-apochromatic objective was used, and emission was collected onto a C9100 Hamamatsu Photonics EM-CCD. CFP was excited with a 440 nm laser, and emission was collected through a 456–484 nm band pass filter. All FRET efficiency was normalized to the mean of the CHX-treated group.

Purification of protein aggregates. 240 ml yeast culture (FlucSM–GFP or FlucSM–GFP–3×Flag) with an optical density around 0.5 were heat shocked in a 42 °C water bath or treated with 0.7 mM H_2O_2 for the desired period of time. After heat shock or H_2O_2, CHX and CCCP were added to prevent aggregate formation and dissolution. Cells were collected by centrifugation at 5,000*g* for 2 min and the pellet was washed once with water, re-suspended in 1 ml 10 mM DTT (100 mM Tris-H_2SO_4, pH 9.3) for 5 min at 30 °C. Then the cells were washed once with sorbitol buffer (20 mM K_2HPO_4/KH_2PO_4, pH 7.5, 1.2 M sorbitol), followed by 5 min digestion with 0.7 mg/ml zymolase100T (US Biological) in 1 ml zymolyase buffer. Zymolyase was removed by centrifugation (800*g*) and cells were washed twice with zymolyase buffer. Cells were lysed with 800 μl ice-cold lysis buffer (50 mM HEPES pH 7.5, 150 mM NaCl, 1 mM DTT, 5% glycerol, 1% Triton-X100 and protease inhibitor cocktail (roche #11836170001) and 10 U/ml RNasin plus RNase inhibitor (N2611) by pipetting 15–20 times on ice. Centrifugation at 800*g* for 2 min was followed by 1 min 6,000*g* centrifugation to remove cell debris. The supernatant was carefully transferred to the top of a sucrose gradient consisting of 650 μl 50%, 2 ml 20% and 1 ml 10% sucrose dissolved in lysis buffer. Samples were centrifuged at 20,000*g* for 16 min. 18-gauge needles were inserted into the 20% sucrose fraction from the side of the centrifuge tube to collect about 900 μl 20% sucrose fraction. The entire 900 μl 20% fraction was applied directly to a column prefilled with about 600 μl M2 resin (A2220, Sigma) prepared in cold room according to the manufacturer's instructions. The column was then washed 20 times with 1 ml cold wash buffer (1 × TBS containing 10 U/ml RNasin plus). Then the beads were carefully transferred into a new 2 ml tube, gently inverted 10–15 times and left on a rack for about 5–10 min to separate the beads from the wash buffer. The supernatant was replaced with fresh wash buffer. The beads were then loaded back into the column and incubated with 650 μl 1 × TBS supplemented with 2% SDS for 5 min on the bench before elution. To examine Tom70 and Tom40 in the purified aggregates, we engineered an HA tag to the C termini of Tom40, Tom70, Om45, Mdm10 and Mdm34 in a FlucSM–GFP–3×Flag background, and of Tom40 and Tom70 in a FlucSM–GFP background. Similar amounts of aggregates purified from seven different strains were used to detect Tom70 and Tom40.

MudPIT analysis. TCA-precipitated proteins were urea-denatured, reduced, alkylated and digested with endoproteinase Lys-C (Roche) followed by modified trypsin (Promega)[37,38]. Peptide mixtures were loaded onto 250-μm fused silica microcapillary columns packed with strong cation exchange resin (Luna, Phenomenex) and 5 μm C18 reverse phase (Aqua, Phenomenex), and then connected to a 100-μm fused silica microcapillary column packed with 5 μm C18 reverse phase (Aqua, Phenomenex)[37]. Loaded microcapillary columns were placed in-line with a Quaternary Agilent 1100 series HPLC pump and a LTQ linear ion trap mass spectrometer equipped with a nano-LC electrospray ionization source (ThermoScientific). Fully automated 10-step MudPIT runs were carried out on the electrosprayed peptides, as described[37]. Tandem mass (MS/MS) spectra were interpreted using SEQUEST[39] against a database consisting of 6,019 non-redundant yeast proteins (NCBI, 2013-02-26 release), 160 usual contaminants (human keratins, IgGs, and proteolytic enzymes). To estimate false discovery rates (FDRs), the amino acid sequence of each non-redundant protein entry was randomized to generate a virtual library. This resulted in a total library of 12,038 non-redundant sequences against which the spectra were matched. Peptide/spectrum matches were sorted and selected using DTASelect[40] with the following criteria set: spectra/peptide matches were retained only if they had a DeltCn of at least 0.08, and minimum XCorr of 1.8 for singly, 2.0 for doubly, and 3.0 for triply charged spectra. In addition, peptides had to be fully tryptic and at least 7 amino

acids long. Combining all runs, proteins had to be detected by at least two such peptides, or one peptide with two spectra. Peptide hits from multiple runs were compared using CONTRAST[40]. To estimate relative protein levels, we calculated distributed normalized spectral abundance factors (dNSAFs) for each detected protein or protein group, as described[41]. Supplementary Tables 1 and 2 were generated by filtering the hits with a stringent cutoff (FDR < 0.05 and identified in 3 out of 4 repeats for 30 min heat shock, 2 out of 2 repeats for other samples). The average dNSAF was used to calculate the percentage of aggregate proteins identified in each condition. The aggregate proteins that could be found in a previously published mitochondrial proteome[42] were included to calculate the percentage of mitochondrial proteins in 30 min heat shock samples.

Mammalian cell culture, transfection and Immunoblots. Human RPE1 cells (ATCC CRL4000, authenticated by ATCC based on Ep-16 antigen as determined by flow cytometry using the Ep-16 monoclonal antibody and cytokeratins as determined by immunocytochemistry using a pan-cytokeratin antibody) were cultured in Dulbecco's Modified Eagle Medium: Nutrient Mixture F-12 (DMEM/F12) (GIBCO), supplemented with 10% (v/v) fetal bovine serum (FBS), 100 IU/ml penicillin. Transient transfections were performed with Lipofectamine 3000 (Invitrogen) according to the manufacturer's instruction. RPE1 cells were double transfected with MTS–mCherry–$GFP_{1–10}$ and the protein of interest tagged with GFP_{11} (2.5 μg of each plasmid was applied). After 24 h of transfection, each sample was equally divided into a new plate and a MatTek (P35G-0-14-C) dish, for western blotting and imaging after another 24 h, respectively. The cell line has been tested and shown to be mycoplasma-negative.

Split GFP assay and quantification. In yeast, proteins of interest were tagged with GFP_{11} at the C termini of their genomic loci in a strain carrying MTS–mCherry–$GFP_{1–10}$. Yeast cells were grown and imaged as described above. Heat shock was performed at 42 °C in 4 ml culture for 30 min with shaking at 220 rpm. 1 ml yeast culture was directly taken out and imaged after heat shock. After heat shock, cultures were shaken at 220 rpm at 30 °C when the indicated time points were acquired (new medium was added to the culture to keep the OD_{600} below 0.5). For CCCP treatment, log phase yeast was treated with 25 μM CCCP at 30 °C for 15 min. For CHX treatment, log phase yeast was treated with 100 μg/ml CHX at 30 °C for 30 min. All images were acquired with the same laser and exposure settings. RPE1 cells were double transfected with split-GFP constructs as described above. Cells were located using the mCherry channel only.

Quantification of split-GFP fluorescence was done using a custom python code. In brief, after reading the mCherry and GFP channel *z* stacks, the intensities were summed along the *z*-axis. The resulting 2D image in the GFP channel was then subject to random walk segmentation to segment out the yeast cells from background and watershed segmentation to separate adjacent cells. The segmentation algorithms were taken from the scikit image library. After segmentation, the median GFP and mCherry intensities in each cell were calculated. Cells whose median GFP was significantly superior to the five cells with lowest GFP in the image were eliminated from further analysis, as they correspond to the autofluorescence of dying cells. For each cell, the mCherry channel was thresholded at 5% of maximal value in order to detect mitochondria, and median GFP intensity within mitochondria was calculated. This median GFP intensity and mCherry intensity were used in the following analyses.

For quantification of the fraction of yeast cells that had the split-GFP signal, all images were acquired with same microscopy settings. Different time points for each sample were set with the same minimum and maximum display values. Maximal *z*-projection images were used to count the number of total cell and cells with distinct split-GFP signals that co-localized with mitochondrial mCherry signals. At least nine fields from three different experiments were quantified at each time point. When cells that had been recovered from frozen glycerol stocks were used, about 5% of yeast in the FlucSM–GFP_{11} samples showed a nuclear GFP signal but not an mCherry signal. These cells were eliminated from quantification in both cell counting and GFP/mCherry intensity ratio quantification.

Quantification of cells with intact mitochondria. Quantification of intact mitochondria was performed using a custom analysis pipeline. The global Otsu threshold was applied to the maximum projection of the mCherry channel to identify the locations of mitochondria and the resulting binary mask was then segmented to determine projections of individual mitochondria. Next, each binary label corresponding to an individual mitochondrion was skeletonized by morphological thinning in order to qualify its morphological structure (circular fragments of mitochondria versus elongated mitochondria). Then, for every binary label, the length of the skeleton and total area covered was computed and used as a basis to classify the region it spanned as either intact mitochondria or fragmented mitochondria. Skeletons longer than 20 pixels or with a total area larger than 25 pixels were used as a cutoff for intact mitochondria.

Code availability. The custom python code for quantification of split-GFP fluorescence and for quantification of intact mitochondria can be found within the git repository at https://github.com/RongLiLab/image_analysis_and_quantification/blob/master/Ruan_Zhou_2016_zstack_analysis.py.

APEX experiment. GFP–APEX2 was cloned from a plasmid from A. Y. Ting's laboratory and the following protocol was derived from the original protocol for mammalian cell culture[43]. MTS–GFP–APEX2 was introduced into the *TRP1* locus of strains expressing HA-tagged cytosolic proteins identified in aggregates. 4 ml of the mid-log culture was heat-shocked for 30 min at 42 °C. The cell wall was reduced by incubating with 10 mM DTT (pH 9.5) for 5 min and cells were washed with zymolyase buffer (pH 7.5, 0.6 M sorbitol, 150 mM NaCl). After the cells were re-suspended in zymolyase buffer, zymolyase (0.2 mg/ml), saponin (0.5 mg/ml) and biotin-phenol (BP) (500 μM) were added for 10 min to remove the cell wall and permeabilize the plasma membrane to allow BP to access mitochondria. The completion of cell permeablization was verified microscopically. H_2O_2 (1 mM) was added for 1 min to activate biotinylation of the mitochondrial proteome by APEX2. Cells were then washed three times with reducing buffer (10 mM sodium ascorbate, 5 mM trolox and 10 mM sodium azide in zymolyase buffer) to stop biotinylation and remove free BP. In this step, the pellet fraction containing organelles, including mitochondria, was separated from cytosolic proteins by centrifugation. After the organelles were re-suspended in 100 μl zymolyase buffer, 1 ml cold lysis buffer (20 mM HEPES, 150 mM NaCl, 1 mM DTT, 1% Triton-X100 and 1× protein inhibitor (04693159001 Roche)) was added to lyse the cells for 5 min on ice. After centrifugation for 10 min at 15,500*g*, the lysate was incubated for 30 min at room temperature with streptavidin magnetic beads (Dynabeads M-280, 11205D) prepared according to the manufacturer's instruction and washed 5 times for 5 min each with PBS supplemented with 0.1% tween-20 and 1 mg/ml BSA. The biotinylated proteins were released from beads by incubating with sample buffer (1× NuPAGE sample buffer (NP0007) supplemented with 20 mM DTT and 2 mM D-biotin) for 10 min at 95 °C.

Mitochondrial isolation and *in vitro* import assay. Mitochondrial purification was based on a previous protocol[44]. In brief, yeast cells expressing MTS–mCherry (in wild-type or $tim23^{ts}$ background) were cultured in 10 l lactate medium (3 g/l yeast extract, 0.5 g/l glucose, 0.5 g/l $CaCl_2$-H_20, 0.5 g/l NaCl, 0.6 g/l $MgCl_2$-$6H_20$, 1 g/l KH_2PO_4, 1 g/l NH_4Cl, 22 ml/l 90% lactic acid, adjusted to pH 5.5 with NaOH) to an OD_{600} of 1. Cells were collected by centrifugation and treated with Tris-DTT buffer (0.1 M Tris, 10 mM DTT, adjusted pH to 9.4). After washing with SP buffer (1.2 M sorbital, 20 mM KPi, pH 7.4), cells were treated with 0.5 mg/ml zymolase100T (US Biological) at 30 °C for 40 min. Spheroplasts were pelleted, washed with the SP buffer, and then resuspended in regeneration buffer (1.2 M sorbitol, 1 × lactate medium without glucose) in order to isolate robust mitochondria. For the protease protection assay, the regeneration step was omitted. Spheroplasts were then washed with SEH buffer (0.6 M sorbital, 20 mM HEPES-KOH pH 7.4, 2 mM $MgCl_2$, 1 mM EGTA pH 8.0, protease cocktail (P2714, Sigma), 10 μM benzamidine-HCl (B6506), 1 μg/ml 1,10-phenanthroline (P9375), PMSF 1 mM was added before use) and broken with a Dounce homogenizer. The homogenate was centrifuged at 1,500*g* (low speed) for 5 min at 4 °C. Supernatant was collected and centrifuged at 12,000*g* (high speed) for 10 min at 4 °C. This step was repeated by resuspending the first low-speed pellet and breaking it with Dounce again. The homogenate was centrifuged at low speed and high speed as described above. The high-speed pellet was collected and the Dounce homogenization was repeated with a loose-fitting pestle. The final high-speed pellet containing crude mitochondria was carefully transferred to a Nycodenz gradient in Beckman 14 × 89 mm Ultra-Clear centrifuge tubes (344059). The gradient consisted of 2.1 ml 25%, 2.1 ml 20%, 2.1 ml 15%, 2.1 ml 10%, and 2.1 ml 5% Nycodenz from bottom to top. The gradient was ultracentrifuged in a swinging bucket rotor (Beckman SW41 rotor) for 60 min at 4 °C at 30,000 rpm. Mitochondria were concentrated around 16% Nycodenz and appeared as a wide red-brownish band in the fourth layer from the top.

Aggregates were purified based on the method described above but with two changes. First, the strains used here (both wild-type and *hsp104* deletion background) expressed FlucSM–HA–GFP–3×Flag–3×FKBP–Myc. The motif 3×FKBP was originally included because we thought induced binding might have been necessary for import of aggregate proteins *in vitro*, but we found that aggregates naturally bind mitochondria without any artificial method (Extended Data Fig. 3c). Second, we used the crude aggregate fraction from the sucrose gradient without affinity purification in order to obtain sufficient free aggregates for the *in vitro* import assay. The mitochondria import assay *in vitro* was as described previously[45]. In brief, purified mitochondria (10 mg/ml) were pre-treated with protease inhibitor cocktail (Sigma P2714, Cell Signaling Technology 5872S) for 15 min and mixed with aggregates in import buffer (3% w/v fatty acid-free BSA, 250 mM sucrose, 80 mM KCl, 5 mM $MgCl_2$, 2 mM KH_2PO_4, 10 mM MOPS-KOH, pH 7.2, 10 μM ATP). We note that the ATP requirement in our assay was much lower than that in previous work[46,47]. This could be due to possible ATP production by the mitochondria in the assay, leading to increased ATP levels that are sufficient to

support Hsp104 activity, or due to a different mechanistic action of Hsp104 in our assay system. The aggregate/mitochondria volume ratio was 1:10 (3 μl 125 μg/ml aggregates from sucrose gradient to 30 μl 10 mg/ml mitochondria). Aggregate concentration was measured and adjusted by BCA assay (Thermo Scientific #23225) and confirmed by imaging of GFP-labelled FlucSM puncta densities. The same amount of mixture was taken out at indicated time points up to 1.5 h and boiled for 15 min in SDS sample buffer for immunoblotting analysis.

Protease protection assay. Mitochondria from the strain expressing FlucSM–HA were purified as described above after heat shock at 42 °C. The only difference was that there was no regeneration step after inducing spheroplasts. Purified mitochondria were washed three times with import buffer without ATP (3% w/v fatty acid-free BSA, 250 mM sucrose, 80 mM KCl, 5 mM $MgCl_2$, 2 mM KH_2PO_4, 10 mM MOPS-KOH, pH7.2) to remove the protease inhibitor. Then the mitochondria were spun down at 4 °C, 13,000 rpm for 10 min. Mitochondria were resuspended and the same amount was added to four different 1.5-ml tubes. Group 1 was used as untreated total mitochondria. Group 2 was treated with trypsin for 1 h at room temperature and then with protease K for another 1 h at room temperature to assess protection by the mitochondrial outer membrane. Group 3 was treated with digitonin to permeabilize the outer membrane and Group 4 was treated with both digitonin and Triton-X100 to permeabilize the inner membrane. Then, Groups 3 and 4 underwent the same protease treatment as Group 2. The volume difference was equalized with SEH buffer. Immediately after the treatment, all the samples were treated with PMSF and boiled for 15 min in SDS sample buffer for immunoblotting analysis.

CHX chase assay. Log phase yeast expressing FlucSM–HA in the *TIM23* and *tim23*^{ts} backgrounds or expressing FlucSM–HA or Lsg1–HA in the *Δpdr5* background were heat-shocked at 42 °C for 30 min. Recovery at 30 °C (23 °C for *tim23*^{ts} groups) was performed in the presence of 100 μg/ml CHX and indicated drugs (50 μM CCCP, 1 mM PMSF, 80 μM MG132). At the indicated time points, the same amount of yeast cells was collected and lysed followed by 15 min boiling in SDS sample buffer and subjected to immunoblotting analysis.

Yeast growth assays. Three single colonies of wild-type cells and *pim1*^{S1015A}:*PIM1* cells were inoculated in YPD and YPG (YP plus glycerol) media at 30 °C overnight. The cultures were then diluted to the same OD of 0.075 to refresh for 3 h at 30 °C in order to enter log phase. Then the OD-adjusted wild-type cells and *pim1*^{S1015A}:*PIM1* cells were plated on YPD and YPG plates. Cells were spotted at 10× serial dilutions from left to right and cultured at 30 °C for 44 h on YPD plates and 60 h on YPG plates before scanning.

Structured illumination microscopy. The mitochondrial outer membrane was labelled with mCherry–Fis1TM. $GFP_{1–10}$ was fused with the mitochondrial matrix protein Grx5 (Grx5–$GFP_{1–10}$). The native aggregate protein Lsg1 was tagged with GFP11. After 30 min heat shock at 42 °C, the split GFP signal was imaged in mitochondria using a Nikon structured illumination microscope (Nikon, N-SIM) with 100× TIRF objective. 3D reconstruction was done using Elements N-SIM software.

Statistical analysis. Statistical analysis was performed with Prism 6.0. For the yeast cell data, unpaired Student's *t*-test was used to determine significant differences between samples. For the mammalian cell imaging data, Dunn's multiple comparisons test (nonparametric distribution) was used to determine significant differences between samples; for the mammalian cell immunoblot results, Tukey's multiple comparisons test (nonparametric distribution) was used to determine significant differences between samples (significance levels: $*P < 0.05$, $**P < 0.01$, $***P < 0.001$). No statistical methods were used to predetermine sample size. The experiments were not randomized and the investigators were not blinded to allocation during experiments and outcome assessment.

Data availability statement. All data generated or analysed during this study are included in this published article (and its Supplementary Information files). All original data generated by authors from Stowers Institute may be accessed from the Stowers Original Data Repository at http://www. stowers.org/research/publications/LIBPB-1150.

31. Longtine, M. S. *et al.* Additional modules for versatile and economical PCR-based gene deletion and modification in *Saccharomyces cerevisiae*. *Yeast* **14,** 953–961 (1998).
32. Mumberg, D., Müller, R. & Funk, M. Yeast vectors for the controlled expression of heterologous proteins in different genetic backgrounds. *Gene* **156,** 119–122 (1995).
33. Huh, W. K. *et al.* Global analysis of protein localization in budding yeast. *Nature* **425,** 686–691 (2003).
34. Tran, P. T., Paoletti, A. & Chang, F. Imaging green fluorescent protein fusions in living fission yeast cells. *Methods* **33,** 220–225 (2004).
35. Zhou, C. *et al.* Motility and segregation of Hsp104-associated protein aggregates in budding yeast. *Cell* **147,** 1186–1196 (2011).
36. Imamura, H. *et al.* Visualization of ATP levels inside single living cells with fluorescence resonance energy transfer-based genetically encoded indicators. *Proc. Natl Acad. Sci. USA* **106,** 15651–15656 (2009).
37. Florens, L. & Washburn, M. P. Proteomic analysis by multidimensional protein identification technology. *Methods Mol. Biol.* **328,** 159–175 (2006).
38. Washburn, M. P., Wolters, D. & Yates, J. R., III. Large-scale analysis of the yeast proteome by multidimensional protein identification technology. *Nat. Biotechnol.* **19,** 242–247 (2001).
39. Eng, J. K., McCormack, A. L. & Yates, J. R. An approach to correlate tandem mass spectral data of peptides with amino acid sequences in a protein database. *J. Am. Soc. Mass Spectrom.* **5,** 976–989 (1994).
40. Tabb, D. L., McDonald, W. H. & Yates, J. R., III. DTASelect and Contrast: tools for assembling and comparing protein identifications from shotgun proteomics. *J. Proteome Res.* **1,** 21–26 (2002).
41. Zhang, Y., Wen, Z., Washburn, M. P. & Florens, L. Refinements to label free proteome quantitation: how to deal with peptides shared by multiple proteins. *Anal. Chem.* **82,** 2272–2281 (2010).
42. Reinders, J., Zahedi, R. P., Pfanner, N., Meisinger, C. & Sickmann, A. Toward the complete yeast mitochondrial proteome: multidimensional separation techniques for mitochondrial proteomics. *J. Proteome Res.* **5,** 1543–1554 (2006).
43. Lam, S. S. *et al.* Directed evolution of APEX2 for electron microscopy and proximity labeling. *Nat. Methods* **12,** 51–54 (2015).
44. Boldogh, I. R. & Pon, L. A. Purification and subfractionation of mitochondria from the yeast *Saccharomyces cerevisiae*. *Methods Cell Biol.* **80,** 45–64 (2007).
45. Stojanovski, D., Pfanner, N. & Wiedemann, N. Import of proteins into mitochondria. *Methods Cell Biol.* **80,** 783–806 (2007).
46. DeSantis, M. E. *et al.* Operational plasticity enables hsp104 to disaggregate diverse amyloid and nonamyloid clients. *Cell* **151,** 778–793 (2012).
47. Fernández-Higuero, J. A. *et al.* Allosteric communication between the nucleotide binding domains of caseinolytic peptidase B. *J. Biol. Chem.* **286,** 25547–25555 (2011).

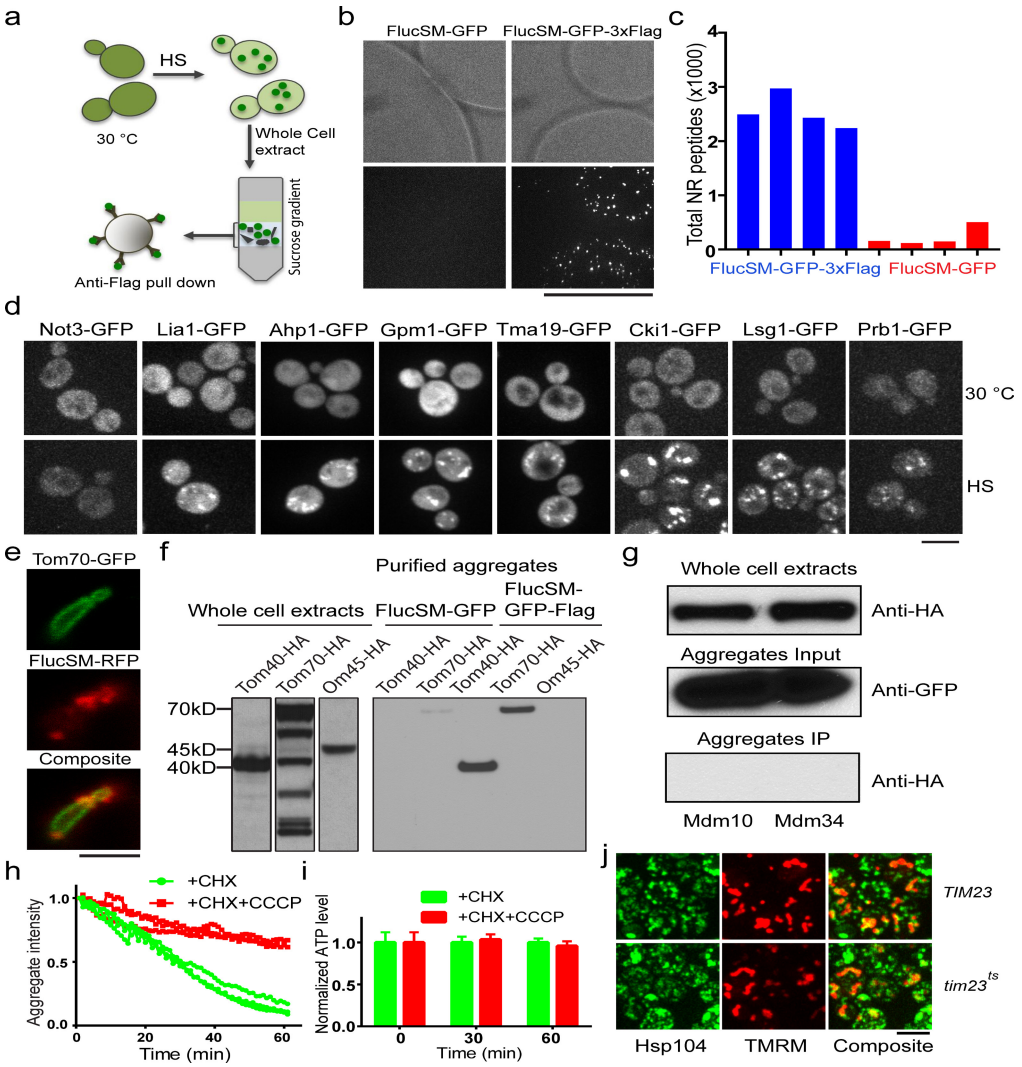

Extended Data Figure 1 | Aggregate purification and role of mitochondrial import in aggregate dissolution. a, Schematics of aggregate purification. Yeast strains expressing FlucSM–GFP–3×Flag or FlucSM–GFP as control were treated with heat shock at 42 °C to induce aggregate formation (green dots). Sucrose gradient centrifugation was then used to separate FlucSM–GFP monomers from aggregates in the cell lysates. The fraction enriched for protein aggregates was applied to an anti-Flag column to separate FlucSM–GFP–3×Flag aggregates from other cellular debris (grey shapes). **b**, Representative images ($n = 8$) of anti-flag resin and associated aggregates isolated from FlucSM–GFP (left) or FlucSM–GFP–3×Flag (right) strains. **c**, Total non-redundant peptides identified by MudPIT of independent repeats using FlucSM–GFP–3×Flag (blue) and FlucSM–GFP (red) strains. **d**, Representative images of examples of proteins identified by MudPIT that form aggregates after 30 min heat shock. Not3 is a negative control. Three images for each. **e**, Tom70–GFP did not colocalize with aggregates after 30 min heat shock. FlucSM–RFP was used as a marker for cytosolic aggregates. Image is representative of five captured. **f**, Anti-HA immunoblot showing co-purification of HA-tagged Tom70 and Tom40 but not Om45 with aggregates. **g**, Additional negative controls for experiment in **f**: anti-HA immunoblotting of two mitochondrial outer membrane proteins Mdm10 and Mdm34 that face the cytosol and were not identified by proteomics to be enriched in aggregates. **h**, Dissolution kinetics of heat shock-induced FlucSM–GFP aggregates in cells treated with CHX (green) or CHX+CCCP (red). Shown are fluorescent traces of three biological repeats for each condition. **i**, Measurement of ATP level under the same experimental conditions as for **h** using a FRET-based sensor showing that CCCP did not deplete cellular ATP. The FRET efficiencies of the CCCP+CHX-treated group and the CHX-treated group were normalized to the mean of the CHX-treated group at each indicated time point. 36 cells were measured at time 0 (before drug addition), 43 and 74 cells for the CHX condition (at 30 and 60 min, respectively), and 39 and 74 cells for CHX/CCCP (at 30 and 60 min, respectively). Shown are means and s.e.m. **j**, Images, representative of about 300 cells imaged, from three biological repeats of *TIM23* and *tim23*^{ts} cells stained with TMRM (red) after heat shock to demonstrate that the membrane potentials of these cells were similar. Scale bar, 2.5 μm for (**e**), 5 μm for other panels. For gel source data, see Supplementary Fig. 1.

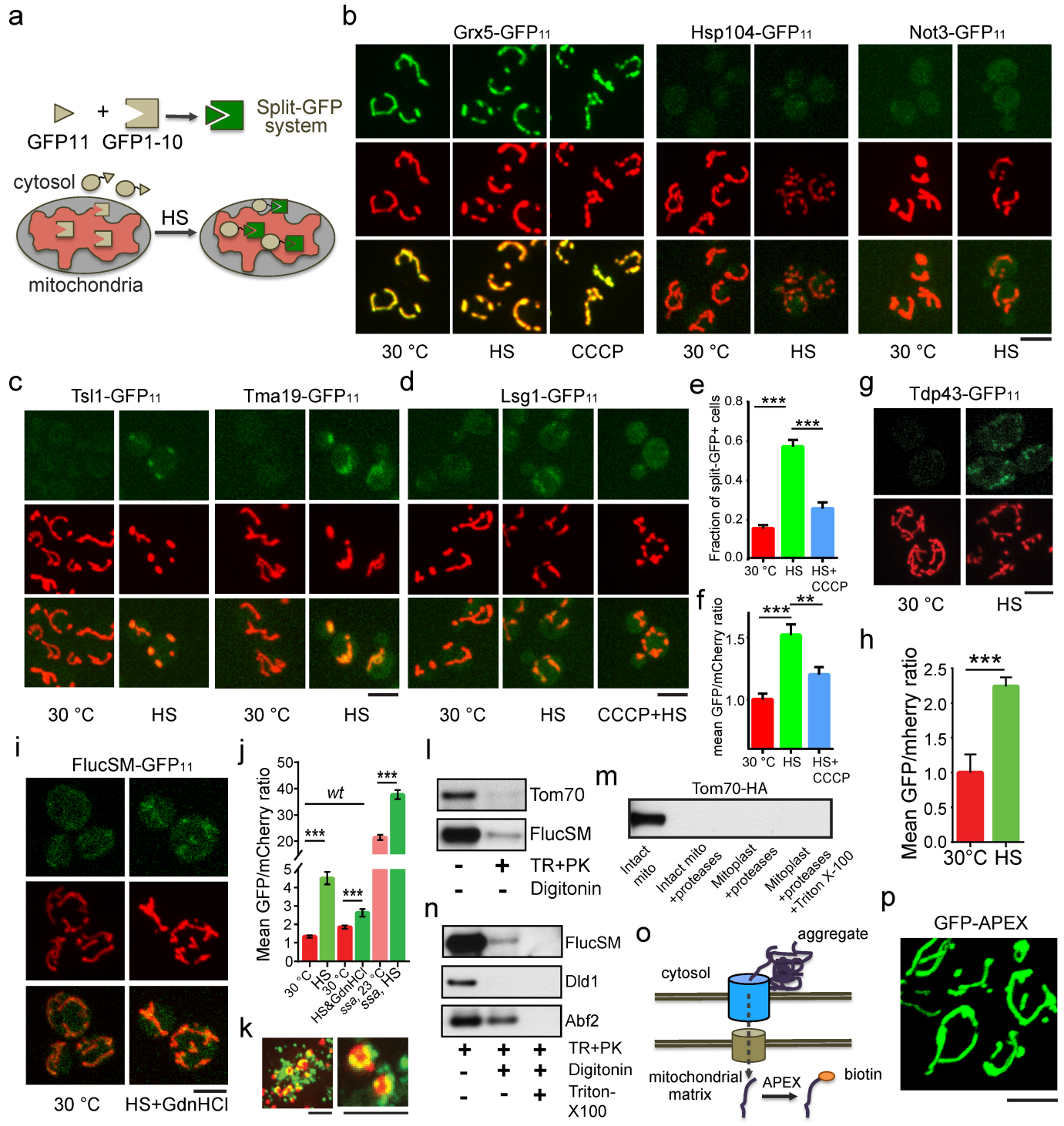

Extended Data Figure 2 | See next page for caption.

Extended Data Figure 2 | Additional data demonstrating import of aggregate proteins into mitochondria after heat shock. a, Schematic diagram explaining the split-GFP assay to detect translocation of a cytosolic protein into mitochondria. **b**, Positive (Grx5) and negative (Hsp104, Not3) controls used for the split-GFP assay. The split-GFP signal for the stable mitochondrial matrix protein Grx5 did not diminish in cells treated at 30 °C with CCCP for 15 min. This result is to be compared with that in Extended Data Fig. 6a. Top, split GFP images; middle, MTS–mCherry-labelled mitochondria; bottom, merged images. Images are representative of 9, 9, 4, 7, 8, 6 and 7 images captured from left to right. **c**, Additional examples of heat shock-induced translocation of cytosolic aggregate proteins into mitochondria, as shown by split-GFP signal after heat shock. Tsl1 and Tma19 are aggregate proteins confirmed by both imaging and proteomics ($n = 9$ from 3 biological repeats). **d**–**f**, Representative images (**d**) and quantifications (**e**, **f**) showing that CCCP treatment blocked the heat shock-induced mitochondrial translocation of Lsg1–GFP_{11}. **e** and **f** show mean and s.e.m. of, from left to right, 874, 503 and 385 cells counted (**e**) and 351, 164 and 261 cells quantified (**f**); three biological repeats. In **f** the intensity ratio from each cell is normalized to the mean of 30 °C control samples before treatment. **g**, **h**, Images (**g**) and quantification (**h**) of TDP43–GFP_{11} split-GFP (top) and mitochondria (bottom). **h** shows mean and s.e.m. of 96 (30 °C) and 133 (heat shock) cells imaged and quantified; three biological repeats. **i**, Representative images showing the effect of inhibition of Hsp104 with GdnHCl on FlucSM import. **j**, Quantification of images in **i** and Fig. 2e with the corresponding controls. Shown are mean and s.e.m., from left to right, of 174, 195, 181, 183, 180 and 168 cells. **k**–**n**, Protease protection assay. **k** shows aggregates with FlucSM–GFP attached to purified mitochondria (red), representative of eight images acquired. **l** and **n** show immunoblots of purified post-heat shock mitochondria treated with or without detergents and proteases as indicated. TR, trypsin; PK, protease K. **m**, Anti-HA immunoblot of Tom70–HA as a mitochondria outer membrane protein in the protease protection assay in various treated samples. **o**, Schematics of the APEX assay to detect mitochondrial import. **p**, Image showing localization of GFP–APEX in mitochondria, representative of three images acquired. Tukey's multiple comparisons test for **e**, **f**; unpaired two-tailed *t*-test for **h**, **j**. $^{**}P < 0.01$, $^{***}P < 0.001$. Scale bars, 5 μm. For gel source data, see Supplementary Fig. 1.

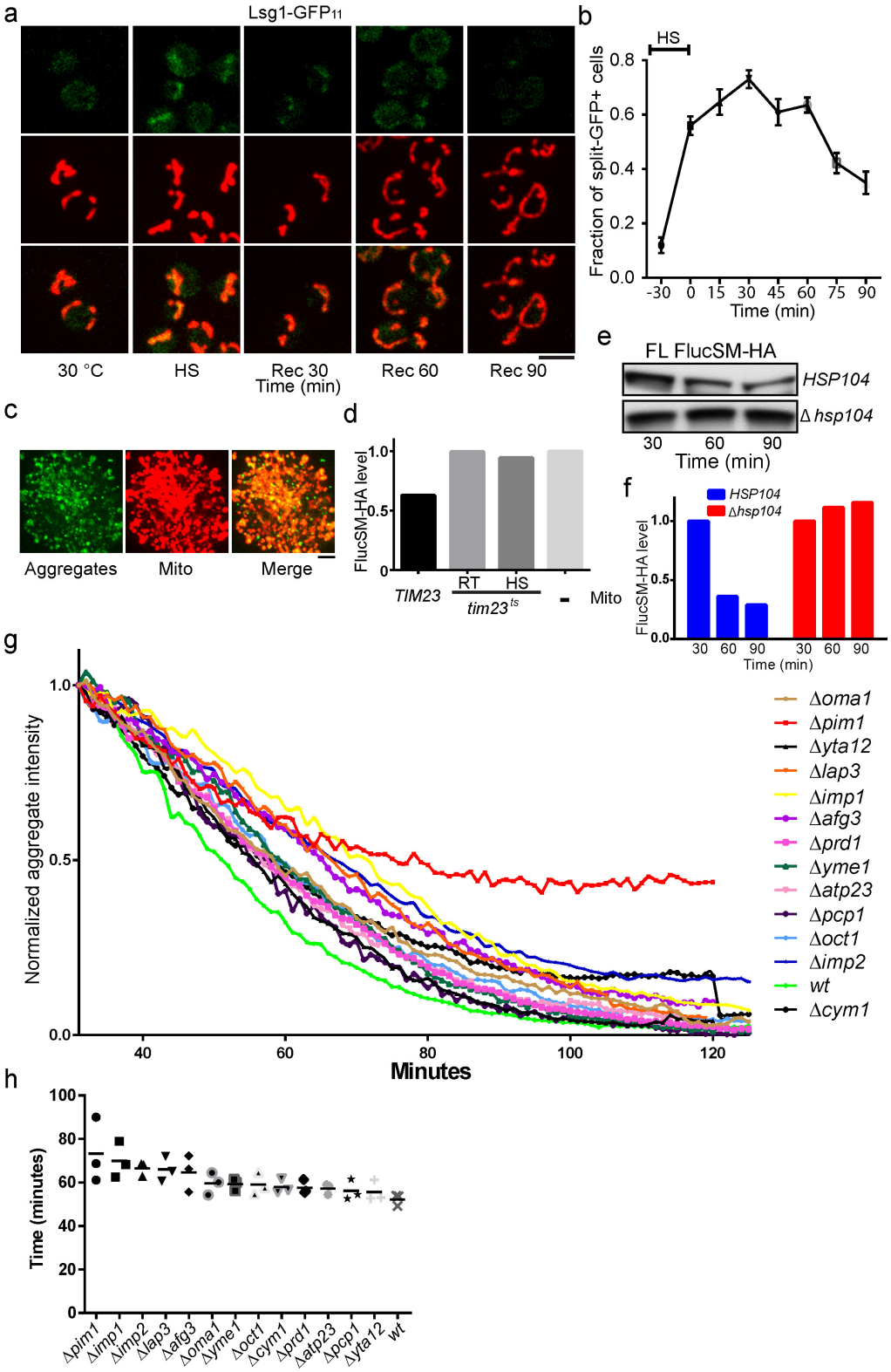

Extended Data Figure 3 | Mitochondrial proteases and peptidases are important for efficient dissolution of aggregates after heat shock. **a**, **b**, Representative images (**a**) and quantification (**b**) over time showing that the mitochondrial split-GFP signal of Lsg1–GFP_{11} increased after 30 min heat shock and gradually diminished during the 90-min recovery after returning to 30 °C. Top, split-GFP images; middle, MTS–mCherry-labelled mitochondria; bottom, merged images. **b** shows the mean and s.e.m. of the fraction of cells from three experiments that had a split-GFP signal at each time point. A total of 2,153 cells were counted; three biological repeats. **c**, Representative images ($n = 8$) of purified aggregates labelled by GFP-tagged FlucSM, bound to purified mitochondria, labelled with MTS–mCherry. **d**, Quantification of the immunoblot shown in Fig. 3c. **e**, **f**, Immunoblots of FlucSM–HA after aggregates purified from *Δhsp104* cells were incubated with wild-type mitochondria for various amounts of time as indicated (**e**) and quantification of the immunoblot (**f**). **g**, **h**, Dissolution curves of aggregates (**g**) and their half-decay times (**h**) showing that the deletion of different mitochondrial proteases delayed the dissolution of cytosolic protein aggregates. **g** shows mean curves; **h** shows data points and mean half decay times extracted from fitted curves of three biological repeats. Original data for each repeat are available in Supplementary Information. Scale bars, 5 μm. For gel source data, see Supplementary Fig. 1.

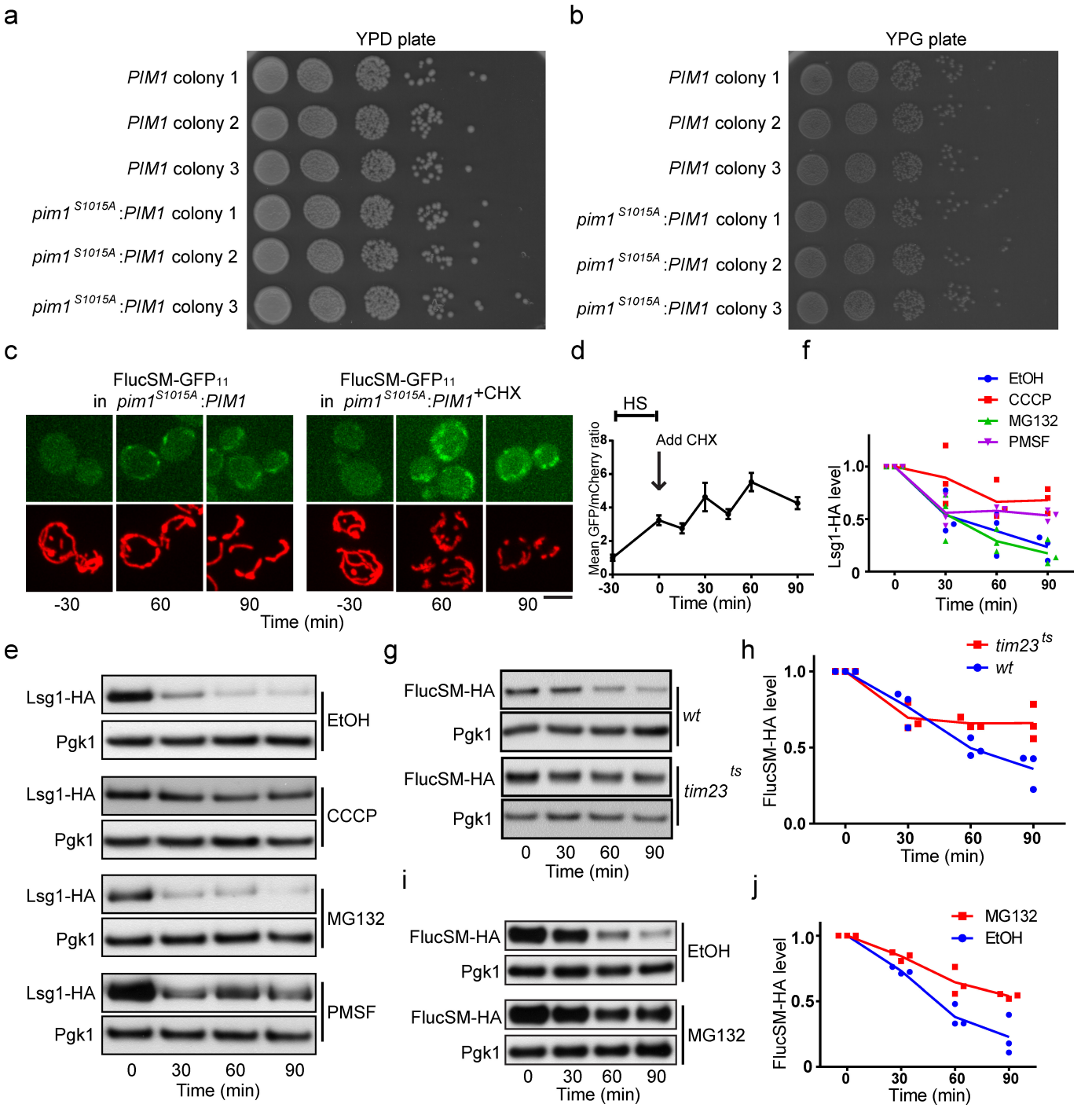

Extended Data Figure 4 | The protease activity of Pim1 is important for efficient degradation of misfolded cytosolic proteins. **a**, **b**, *pim1*^{S1015A}:*PIM1* grows normally under fermentable (**a**) and non-fermentable conditions (**b**). **c**, Representative images showing that delayed split-GFP of FlucSM disappearance in *pim1*^{S1015A}:*PIM1* cells was not affected by CHX during the recovery phase. Top, split GFP images; bottom, MTS–mCherry-labelled mitochondria. **d**, Quantification of mean split-GFP/mCherry ratio for *pim1*^{S1015A}:*PIM1*. CHX was added after heat shock. Plotted are mean and s.e.m. from 747 cells that were imaged and measured; three biological repeats. **e**, **f**, Representative immunoblots (**e**) and quantification (**f**) from three biological repeats showing that the mitochondrial import (inhibited by CCCP) is the major source for degrading stress-damaged endogenous Lsg1–HA, but vacuole-mediated degradation (inhibited by PMSF) also plays a role, while the proteasome pathway (inhibited by MG132) has the least effect. **f** shows data points and mean. **g**, **h**, Representative immunoblots (**g**) and quantification (**h**) of wild-type or *tim23*^{ts} cells treated with CHX after heat shock showing that mitochondrial import (inhibited by *tim23*^{ts}) is important for the degradation of stress-damaged FlucSM–HA. **h** shows data points and mean plots from three biological replicates. **i**, **j**, Representative immunoblots (**i**) and quantification (**j**) showing that without heat shock, proteasome-mediated degradation of FlucSM–HA was inhibited by MG132. **j** shows data points and mean plots from three biological replicates. Scale bar, 5 μm. For gel source data, see Supplementary Fig. 1.

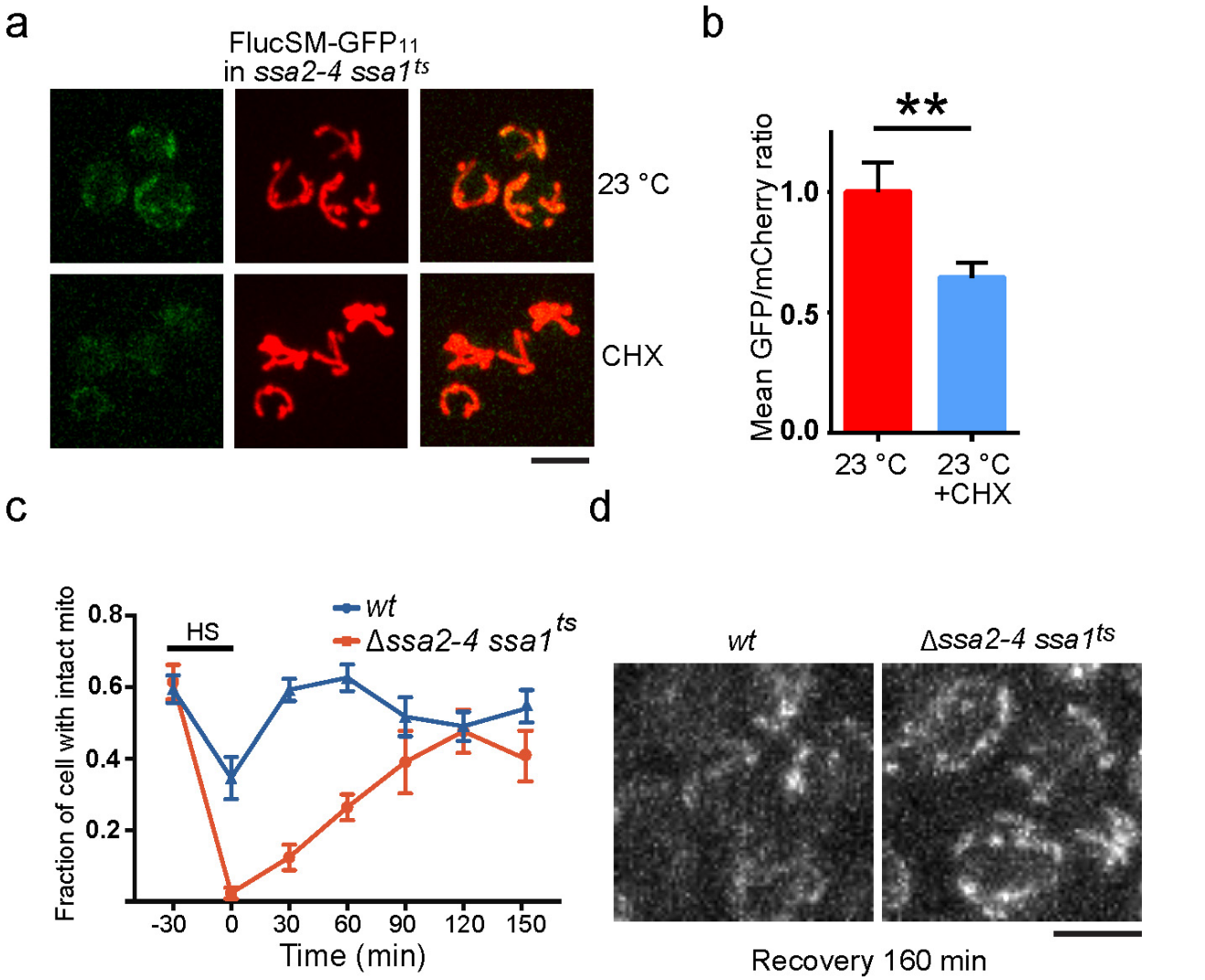

Extended Data Figure 5 | Impairment of cytosolic Hsp70 leads to enhanced import of unfolded proteins into mitochondria and mitochondrial damage. a, **b**, Representative images (**a**) and quantification (**b**) of split-GFP signal for FlucSM–GFP_{11} in the *Δssa2 Δssa3 Δssa4 ssa1*^{ts} strain. Cells growing at 23 °C were treated with CHX for 30 min. Shown are mean and s.e.m. of 126 and 133 cells imaged and measured; three biological repeats. Unpaired two-tailed *t*-test: $^{**}P < 0.01$. **c**, The fraction of cells with intact mitochondria was decreased after heat shock and the *Δssa2 Δssa3 Δssa4 ssa1*^{ts} mutant showed more severe fragmentation and delayed recovery compared to the wild type (see also representative mitochondrial images in Fig. 3a). Shown are mean and s.e.m. quantified from three biological repeats with 1,335 cells for the wild type and 967 cells for the mutant. **d**, Representative images (from the 160-min time point of the plot in Fig. 3h) of ROS indicated by DHE signal. 1,621 mutant and 2,151 wild-type cells were imaged and quantified. Scale bars, 5 μm.

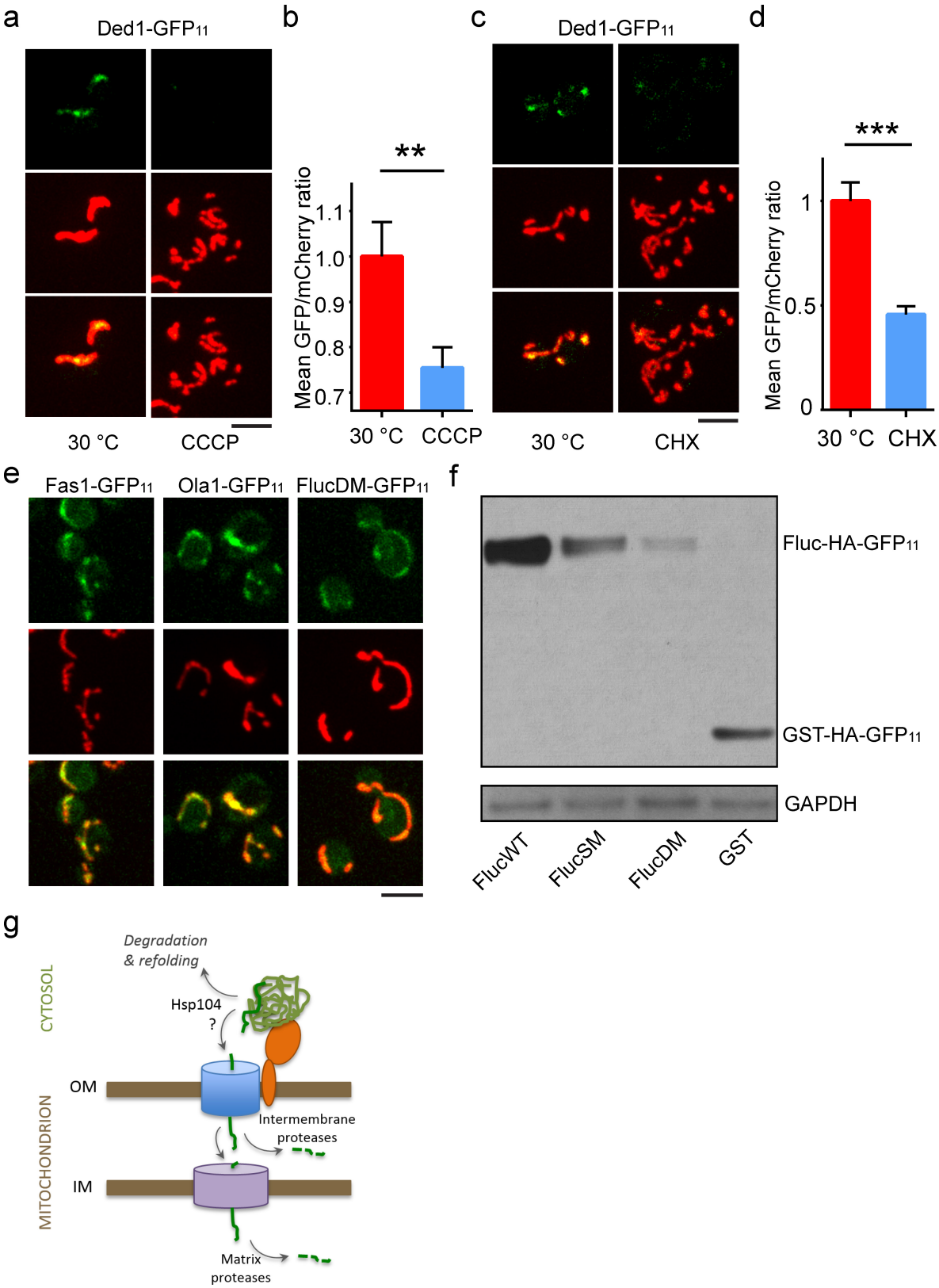

Extended Data Figure 6 | See next page for caption.

Extended Data Figure 6 | Unstably folded cytosolic proteins are imported into mitochondria in both yeast and human RPE1 cells. **a**–**d**, Representative images (**a** and **c**) and quantification (**b** and **d**, as in Fig. 2c) of the split-GFP signal for the super-aggregator Ded1 in cells grown at 30 °C without or with CCCP for 15 min or without or with treatment with CHX for 30 min at 30 °C, with 205 and 182 cells imaged and quantified in **a**, **b**, respectively; 283 and 287 cells imaged and quantified in **c**, **d**, respectively; three biological repeats. Top, split GFP images; middle, MTS–mCherry-labelled mitochondria; bottom, merged images. **b** and **d** show mean and s.e.m. of measurements from the indicated number of cells. Unpaired two-tailed *t*-test: $^{**}P < 0.01$, $^{***}P < 0.001$. **e**, Images of the split-GFP signal of cells expressing the super-aggregators Fas1–GFP_{11}, Ola1–GFP_{11} or FlucDM–GFP_{11} under non-stressful growth conditions (30 °C) showing that these proteins are imported into mitochondria even without imposed proteotoxic stress. Top, split GFP images; middle, MTS–mCherry-labelled mitochondria; bottom, merged images. $n = 7$, 9 and 9 from left to right. **f**, Immunoblot showing expression of different luciferase mutants relative to wild-type luciferase in human RPE1 cells (corresponding to the quantification in Fig. 4c), representative of five biological repeats for the Fluc proteins. Loading control, GAPDH. **g**, Working model of MAGIC. Cytosolic aggregates are attached to mitochondria through interaction with import receptors such as Tom70. Individual aggregate proteins, which may be dissociated from aggregates by Hsp104, are imported through the outer membrane import complex to the intermembrane space, where they are either degraded by intermembrane proteases and peptidases, or imported through an inner membrane channel to be degraded by matrix proteases such as Pim1. Scale bars, 5 μm. For gel source data, see Supplementary Fig. 1.